THE ASTROPHYSICAL JOURNAL, 471:447–453, 1996 November 1

PULSE PHASE–DEPENDENT SPECTROSCOPIC STUDY OF VELA X-1

C. S. CHOI,[1] T. DOTANI,[2] C. S. R. DAY,[3] AND F. NAGASE[2]

Received 1995 September 26; accepted 1996 May 13

ABSTRACT

We analyzed the X-ray observations of Vela X-1 obtained with the *Ginga* large area counter (LAC) on 1991 August 18–19. During the observations, which cover orbital phase $\Phi_{orb} = 0.29$–0.47, we detected an intensity dip at $\Phi_{orb} = 0.33$–0.38. The pulse amplitude of the X-ray flux was much reduced in the dip and was almost invisible in lower energy band. From the spectroscopic study, clear modulation of the iron line flux with the pulse period was observed at the half-amplitude of 10% during the dip. We also detected modulation of the iron line center energy in the data set obtained at $\Phi_{orb} = 0.43$–0.47. These phenomena may be explained by the X-ray reprocessing in the accretion wake.

Subject headings: binaries: eclipsing — pulsars: individual (Vela X-1) — X-rays: stars

1. INTRODUCTION

Vela X-1 (4U 0900−40) is an eclipsing binary X-ray pulsar consisting of a neutron star and a massive early-type companion star (HD 77581, B0.5 Ib; Vidal, Wickramasinghe, & Peterson 1973, Conti 1978). Since the discovery of Vela X-1 (Chodil et al. 1967) and the X-ray pulsations (McClintock et al. 1976), its 8.964 day orbital period and 283 s X-ray pulsation have been confirmed by many X-ray observations (see Nagase 1989, and references therein, for details of the system parameters). The X-ray luminosities of Vela X-1, $\sim 10^{36}$ ergs s^{-1}, is explained well by wind accretion from the optical companion. The estimated mass-loss rate is $\sim 10^{-6}\ M_{\odot}\ \mathrm{yr}^{-1}$ (Conti 1978; Dupree et al. 1980; Lewis et al. 1992). In this binary, the large temporal variability of the X-ray intensity of a few minutes to several hours has been ascribed both to fluctuations in the accretion rate and to inhomogeneities in the flow of stellar wind (Watson & Griffiths 1977; Nagase et al. 1983; Haberl & White 1990).

The spectral features of Vela X-1 follow in general the common characteristics of X-ray pulsars, i.e., a conventional power law with an exponential high-energy cutoff and an iron emission line centered at ~ 6.4 keV (Becker et al. 1978; White, Swank, & Holt 1983; Nagase 1989; Gottwald & White 1990). However, the pulse-averaged spectrum of Vela X-1 is highly affected by the absorption of the wind and is variable over the orbital phase (Kallman & White 1982; Nagase et al. 1986). The modifications occur mainly in the soft X-ray range due to changes in the absorption column through the line of sight. These spectral variations together with the line parameters have been used as a useful tracer of circumstellar matter in X-ray binaries.

The pulse period changes of Vela X-1 have been monitored during the past 20 years, and it has been noted that the long-term behavior shows wavy fluctuations (see, e.g., Nagase et al. 1984a, 1984b; Boynton et al. 1984). The transfer of angular momentum by wind accretion was invoked to account for the reversals of spin-up and spin-down. However, it has been pointed out by several authors that spherical accretion is insufficient to explain the observed pulse period changes because of the small rate of angular momentum transfer (Livio et al. 1986; Soker et al. 1986; Anzer, Börner, & Monaghan 1987). An accretion disk that acts as a reservoir for the momentum transfer has been proposed in order to solve the problem, although the model requires a high magnetic field of $B \sim 10^{13-14}$ G (Börner et al. 1987). Several numerical studies have reproduced not only the formation of such a disk but also dense sheets of matter that may be formed by radiation pressure–driven shocks (Fransson & Fabian 1980; Krolik & Raymond 1985; Börner et al. 1987; Taam & Fryxell 1989, Blondin et al. 1990; Blondin, Stevens, & Kallman 1991; see also Nagase 1989 for a review). In addition to these, a localized emission site for the iron line was suggested from the X-ray observations with the *Tenma* gas scintillation proportional counter (GSPC) (Ohashi et al. 1984; Sato et al. 1986). However, the presence of this matter, including the accretion disk, has not been confirmed observationally. In the present paper, we analyze data acquired from the *Ginga* LAC observation to extract information about matter distribution in the binary system of Vela X-1/HD 77581.

2. OBSERVATION AND RESULTS

The *Ginga* observations of Vela X-1 which we use in this study were made with the LAC from 1991 August 18 4:04 (UT) to August 19 18:47 (UT). The LAC consists of eight proportional counter modules with a total effective area of 4000 cm^2 and covers the energy range of 1–37 keV with an energy resolution of 18.0% at 6 keV. The data were recorded in MPC-1 mode, which covers the above energy range with 48 pulse height channels. Details of the instrument and its performance are given in Turner et al. (1989).

We checked the solar X-ray contamination by referring to the Sun angle, which gives the angle between the LAC pointing direction and the Sun, and by inspecting the spectrum of each counter. As a result, we omitted data obtained from three counter modules (counters 2, 3, and 7) on the right corner of the LAC that appeared to be contaminated by solar X-rays. Therefore, we analyze the data acquired from five counters with a combined effective area of 2500 cm^2. To subtract the background, including contamination of the galactic ridge emission (see, e.g., Koyama et al. 1986), we used the blank sky observation near the Cyg A region ($l \simeq 76\overset{\circ}{.}1$, $b \simeq 5\overset{\circ}{.}8$; the galactic coordinates of Vela X-1 are

[1] Korea Astronomy Observatory, 36-1 Hwaam, Yusong, Taejon 305-348; cschoi@hanul.issa.re.kr.

[2] The Institute of Space and Astronautical Science 3-1-1 Yoshinodai, Sagamihara, Kanagawa 229, Japan; dotani, nagase@astro.isas.ac.jp.

[3] USRA, Laboratory of High Energy Astrophysics, NASA/Goddard Space Flight Center, Code 668, Greenbelt, MD 20771; day@lheavx.gsfc.nasa.gov.

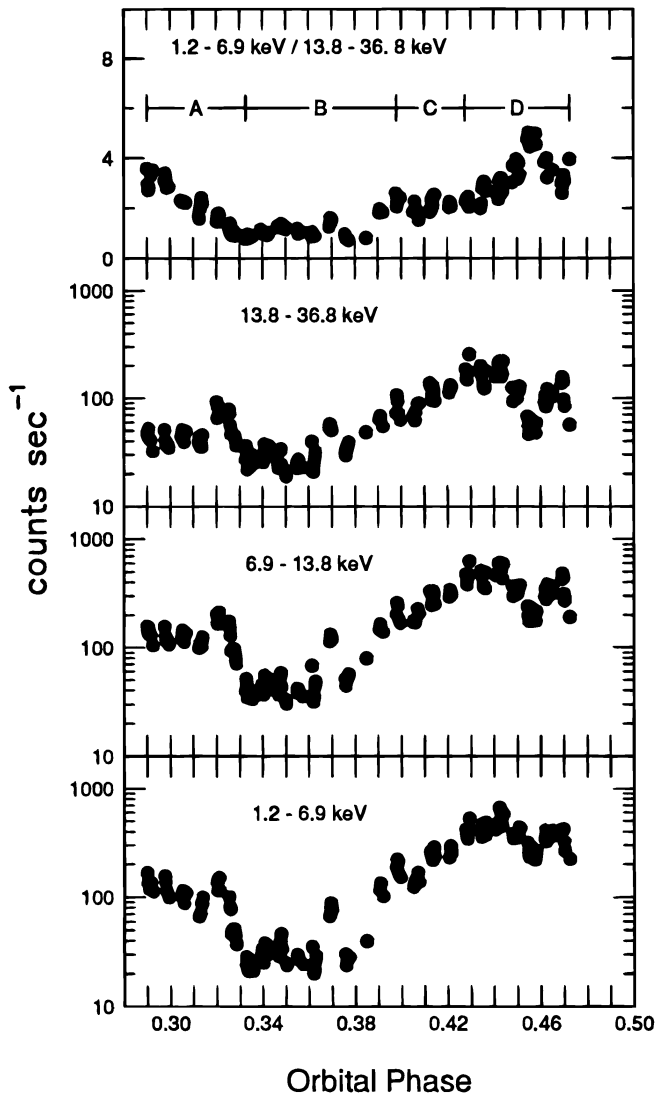

FIG. 1.—X-ray light curves of Vela X-1 in three energy bands observed with *Ginga* LAC on 1991 August 18–19. Each of the plotted points indicates the accumulated data with a time resolution of 240 s after background subtraction, and the typical uncertainty is about 1 count s^{-1}. The top panel is the softness ratio of the two count rates.

$l = 263.^{\circ}07$, $b = 3.^{\circ}93$) measured 1 day earlier than the present observation.

The X-ray light curves taken at three different energy bands and the softness ratio of the flux in 1.2–6.9 keV to that in 13.8–36.8 keV are shown in Figure 1.The orbital phase listed on the figure was calculated using the ephemeris (JD 2,447,210.613) determined by Lewis et al. (1992) and the known orbital parameters (phase zero corresponds to mid-eclipse). As expected from the previous studies of the X-ray variability, the observed count rate shows a considerable change during the observation: from $\sim$0.04 counts cm^{-2} s^{-1} to $\sim$0.4 counts cm^{-2} s^{-1} (1.2–36.8 keV), with a timescale of minutes to hours. The overall pattern of the variation is approximately independent of the energy.

We divide the light curve shown in Figure 1 into four groups to get the pulse phase–dependent spectra at different continuum levels. The pulse profiles in soft (1.2–4.0 keV) and hard (7.5–36.8 keV) bands are plotted in Figure 2 for the four groups. The profiles in A, C, and D are consistent with the typical pulse profiles of Vela X-1 (see, e.g., White et al. 1983; Nagase 1989), i.e., sinusoidal double peaks at high energies and complex five peaks at low energies. On the other hand, the pulsation amplitude is reduced significantly in the dip state (the interval B), even at high energy, and it becomes almost invisible in the lower energy band.

3. SPECTRAL ANALYSIS

The pulse dependency of the Vela X-1 spectrum has not been examined in detail. Although Ohashi et al. (1984) performed phase-resolved spectral analysis of *Tenma* GSPC data, they did not find any pulse modulation of the iron line intensity with an upper limit of about 20%. We attempt first to fit the pulse-averaged spectra with the typical X-ray pulsar spectral model in order to obtain a reference continuum for the phase-resolved spectra. Then, we divide the spectra into 16 pulse phase bins, thus obtaining a total of 64 phase-resolved spectra, and these spectra are analyzed in detail. First we fit the phase average spectra by a model with a power law modified by the cyclotron resonant scattering plus an emission line with a Gaussian (Makishima et al. 1990; Nagase et al. 1991). This model does not contain a sharp structure such as that seen in an exponential high-energy cutoff, and it can reproduce the overall shape of the energy spectrum relatively well. The model spectrum we adopted is

$$f(E) = IE^{-\alpha} \exp\left[-N_{\rm H}\sigma(E) - \frac{D(E/E_1)^2}{(E-E_1)^2 + W^2}\right] + \frac{I_{\rm Fe}}{\sqrt{2\pi}\gamma} \exp\left[-\frac{(E-E_K)^2}{2\gamma^2}\right],$$

where E is the X-ray photon energy, $f(E)$ is a photon number spectrum, I is the normalization, α is the photon index, $N_{\rm H}$ is the hydrogen equivalent column density, $\sigma(E)$ is the photoelectric absorption cross section, E_1 is the electron cyclotron energy, W is the resonance width, D is the depth at the resonance, $I_{\rm Fe}$ is the iron line flux, E_K is the iron line center energy, and γ is the iron line width. The cross section compiled by Morrison & McCammon (1983) was used for $\sigma(E)$. The best-fitting parameter values are listed in Table 1, and the solid lines of Figure 3*a* display the results. The parameters we obtained for the cyclotron resonant scattering may include systematic error because the structure appears very close to the upper bound of the LAC energy range. However, because the systematic errors do not affect the iron line analysis, we do not pursue the systematic errors further. To fit the B spectrum acceptably, we had to employ three column densities. Thus, the model spectrum used to fit the B spectrum is

$$f_B(E) = [I_1 \exp(-N_{\rm H1}\sigma) + I_2 \exp(-N_{\rm H2}\sigma) + I_3]E^{-\alpha} \times \exp\left[-\frac{D(E/E_1)^2}{(E-E_1)^2 + W^2}\right] + \frac{I_{\rm Fe}}{\sqrt{2\pi}\gamma} \exp\left[-\frac{(E-E_K)^2}{2\gamma^2}\right].$$

The weighted average of the line energies of the four data sets is $E_K = 6.46 \pm 0.05$ keV, consistent with previous work. This means that the emission is predominantly produced by fluorescent Kα transition by cold circumstellar matter. The parameter values reveal that the equivalent hydrogen column density of intervening matter is highly variable

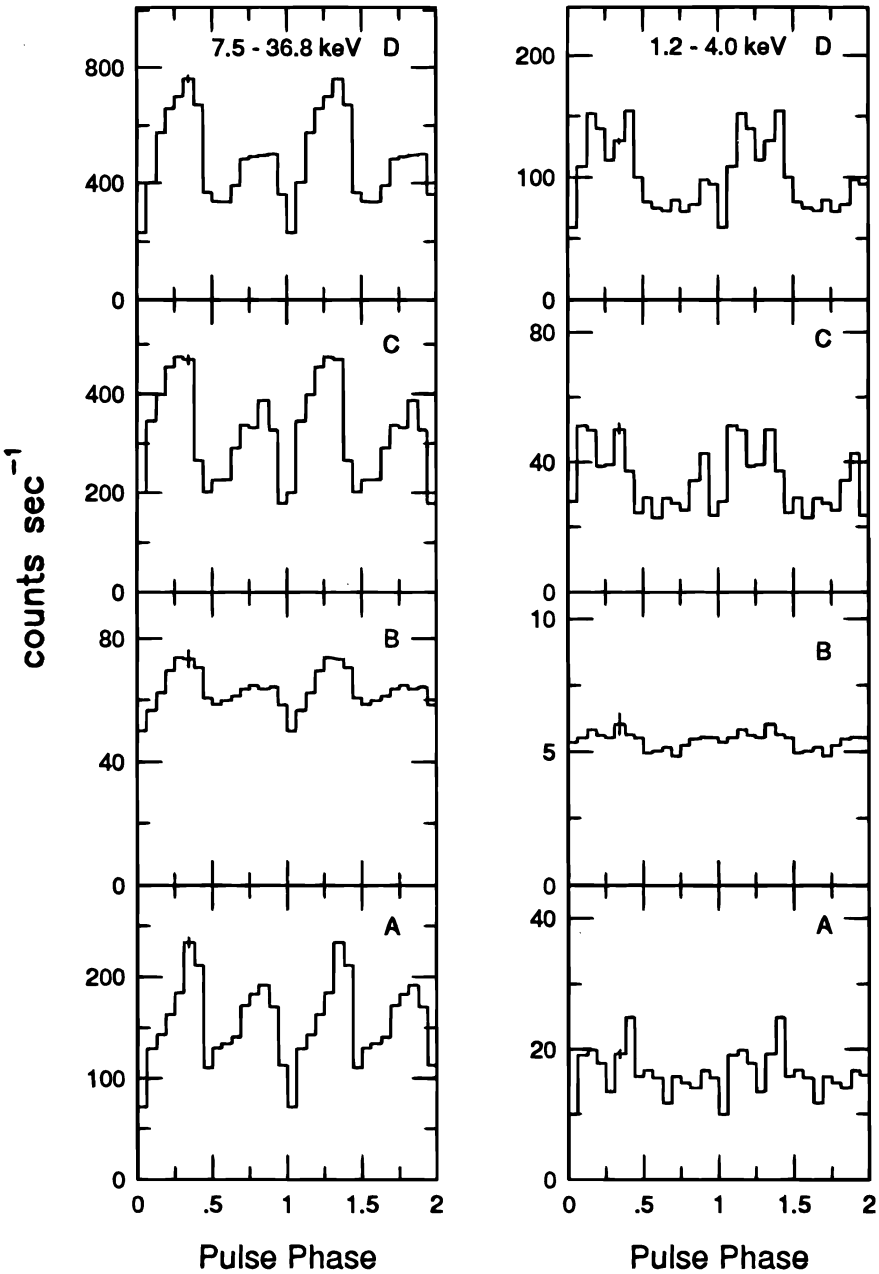

FIG. 2.—Pulse profiles are shown for data sets A through D in two energy bands. Vertical bars in the figure indicate typical 1 σ error.

during observation, from $N_H = 7.5 \times 10^{22}$ cm^{-2} to 2.2×10^{24} cm^{-2}, and that the iron line flux varies from 3.6×10^{-3} photons cm^{-2} s^{-1} to 10.0×10^{-3} photons cm^{-2} s^{-1} while the absorption-corrected continuum above 7.1 keV varies about a factor of 4 in between the data set B and D.

To extract the iron line profile, phase-resolved spectra of each data set were normalized with the model continuum obtained above for the phase-average spectra. Here the model continuum means the first term of $f(E)$, i.e., the power law modified by the photoelectric absorption and cyclotron resonant scattering. The model continuum does not include a line component, and hence the phase-resolved spectra normalized by the model continuum are expected to show the line profile clearly. A mathematical model of a third-order polynomial plus a Gaussian used in the similar study of Her X-1 (see Choi et al. 1994 and also Day et al. 1993 for the method and the model) is also adopted to fit the normalized Vela X-1 spectra in the energy range of 3.4–9.2 keV. We fixed the line width to the value of the phase-averaged one in the course of model fitting. Although this model is not obviously astrophysical, we believe that it allows the reliable estimation of the iron line parameters, since any continuum model that connects smoothly throughout the line region can interpolate reasonably well the continuum flux underlying the iron line. Proportional counters have relatively poor energy resolution so that sharp features, if present in the continuum, cannot be constrained. This means that any smooth continuum can produce a consistent estimation of the line parameters provided we restrict the fitting to a relatively narrow energy region near the iron line. Examples of the normalization and the spectral fit applied to the pulse-averaged spectra are shown in Figure 3*b*, where the dashed line is the polynomial component and the solid line represents the sum, respectively.

Figure 4 shows the plot of the iron line flux against the

TABLE 1

BEST-FITTING PARAMETERS FOR THE PULSE-AVERAGED SPECTRA

Parameter	A	B	C	D
α	1.12 ± 0.01	0.78 ± 0.01	0.95 ± 0.01	0.88 ± 0.03
log N_H (cm^{-2})[a]	23.24 ± 0.01	$24.35 \pm 0.01 (23.48 \pm 0.01)$	23.16 ± 0.01	22.87 ± 0.02
E_1 (keV)	30.2 ± 0.5	32.8 ± 0.5	30.7 ± 1.2	35.6 ± 2.3
W (keV)	2.7 ± 0.2	4.1 ± 0.2	3.0 ± 0.5	5.6 ± 1.4
D	7.8 ± 0.8	8.6 ± 0.7	7.6 ± 2.1	8.6 ± 4.6
I_{Fe} (10^{-3} photons cm^{-2} s^{-1})	4.2 ± 0.3	3.6 ± 0.1	8.8 ± 0.8	10.0 ± 1.4
E_K (keV)	6.36 ± 0.05	6.48 ± 0.02	6.41 ± 0.05	6.58 ± 0.07
Γ[b] ($\equiv 2.35\gamma$; keV)	0.9 ± 0.2	0.6 ± 0.1	0.8 ± 0.2	0.8 ± 0.3
EW[c] (keV)	0.32 ± 0.02	1.31 ± 0.05	0.34 ± 0.03	0.24 ± 0.03
I_c[d] (photons cm^{-2} s^{-1})	1.44	1.02	2.95	4.31
χ^2_ν (dof)	0.86 (20)	1.50 (17)	0.88 (20)	0.71 (20)

NOTE.—All quoted errors represent 90% confidence level for a single parameter.

[a] Continuum of B consists of three power laws of different absorption column; log N_H of the second power law is indicated in the parenthesis. Third power law has no absorption column. See text for the model function.

[b] Intrinsic line width represented by FWHM.

[c] Equivalent width of the iron line.

[d] Continuum flux above 7.1 keV corrected for the absorption using the best-fit parameters.

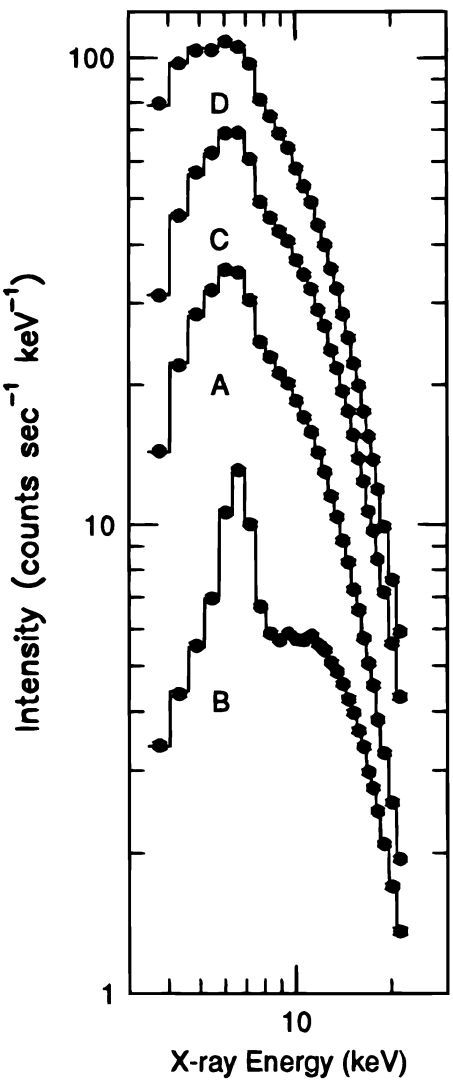

FIG. 3a

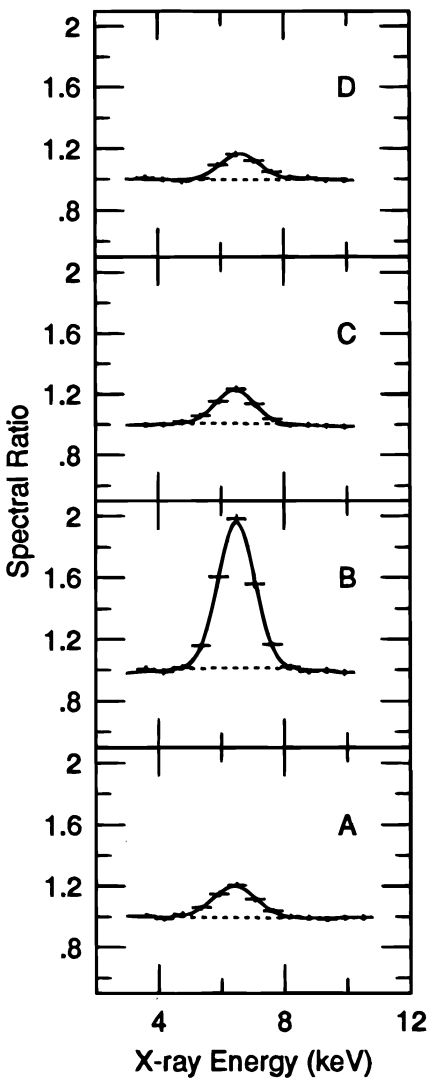

FIG. 3b

FIG. 3.—(*a*) Pulse-averaged energy spectra of Vela X-1 (*filled circles*) and the best-fitting model functions (*solid lines*). Error bars in the spectra are smaller than the symbols. See text for the model functions. (*b*) Examples of the normalized energy spectra (*crosses*) obtained from the pulse-averaged data, and the best-fitting model function (*solid lines*). Dotted line represents the model continuum (see text).

pulse phase, in which the line flux and the pulse amplitude (7.5–36.8 keV) are normalized, respectively, to their average values for each data set. The line flux was derived by integrating the Gaussian profile. From the pulse-dependent spectroscopic study, a sinusoidal modulation of about 10% at half-amplitude is clearly observed in the iron line flux of the dip state data set (B). Other data sets also show erratic variations of the line flux with a half-amplitude of $\sim 10\%$ to $\sim 20\%$. In order to evaluate the statistical significance of the line flux modulation, we need to consider not only the Poisson fluctuation but also the fluctuation intrinsic to the source. It is known that accretion-powered pulsars including Vela X-1 show erratic variations on various timescales other than the coherent pulsation. Such erratic variations may contribute to the iron line modulation in the phase-resolved spectra. Because the pulse phase was divided into 16 bins in the present analysis, erratic variations in the frequency range of 3.53×10^{-3} Hz (pulse frequency) and 5.65×10^{-2} Hz (16 times the pulse frequency) contribute to the iron line modulation. We calculated a power spectrum for each energy bin around the iron line energy and evaluated the power due to the erratic variations in the above frequency range. The ratio, η, of the integrated power due to the erratic variations to the power of the Poisson fluctuation in the same frequency range was almost constant around the iron line energy and was 1.98, 0.07, 1.84, and 2.39 for data sets A, B, C, and D, respectively. When we evaluate statistical significance of the line flux modulation, we can include approximately these erratic variations into the evaluation just by increasing the error bars of the line flux against a constant model using these corrected errors, in which both Poisson and erratic variations are included. The reduced χ^2 values obtained were, respectively, $\chi^2_\nu = 0.50$ (A; dof = 15), 3.90 (B), 0.89 (C), and 0.86 (D). This indicates that data set B has significant flux variations of iron line, but other data sets (A, C, D) do not.

Recently, *ASCA* observed multiple iron lines in the eclipse spectrum of Vela X-1 (Nagase et al. 1994), even though the 6.4 keV line dominates the others in the *ASCA* spectrum. Unfortunately, the present observation cannot resolve the lines. However, we studied the pulse-dependent variations of the line center energy and the results are shown in Figure 5. The line energy of data set D tends to have higher energy at the main peak of the pulse. We checked a possible correlation between the iron line energy and the continuum slope at the line energy. We could not find significant correlations. Furthermore, although the phase-resolved energy spectrum of data set C is very similar to that of the corresponding phase of data set D, no modulation is seen in the line center energy of data set C. Thus, we conclude that the line energy modulation observed in data set D is not an artifact due to the present analysis method. Line energies of the other data sets A, B, and C are consistent with no variations.

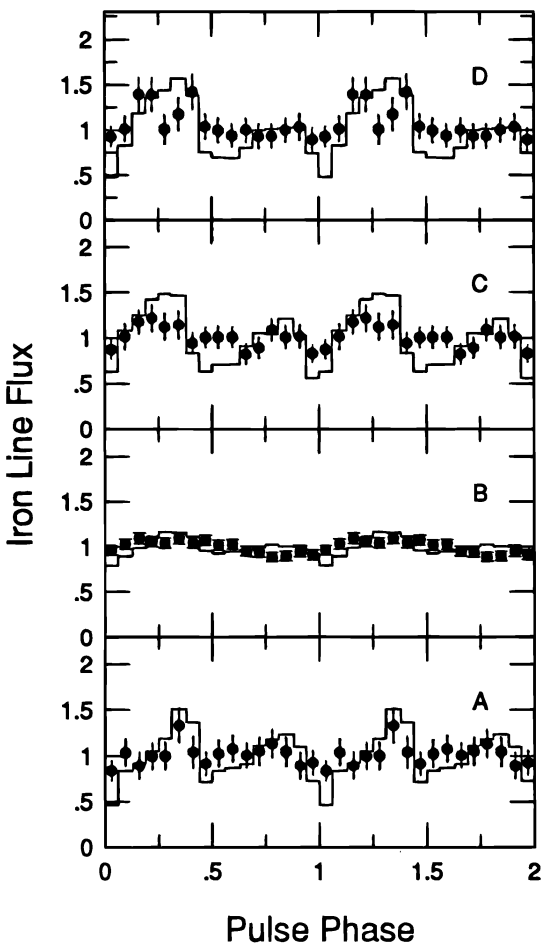

FIG. 4.—Iron line fluxes (*filled circle*) are plotted against the pulse phase. Solid line represents the continuum X-ray flux in 7.5–36.8 keV normalized to the phase-averaged value after background subtraction. All quoted errors in the figure represent only the statistical errors in 90% confidence limit.

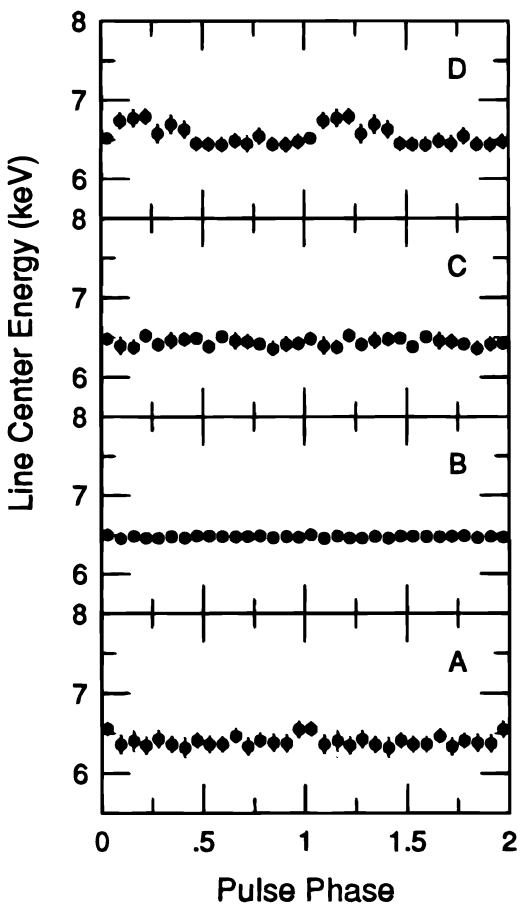

FIG. 5.—Pulse-dependent variations of the line center energy. Error bars in the figure correspond to 90% confidence limit.

4. DISCUSSION

We studied the iron line strength and energy as a function of pulse phase. We found that iron line flux was pulsating for data set B, and that the iron line energy varied with pulse phase for data set D. This means that the reprocessing material responsible for the line emission cannot be isotropic. The data we analyzed here covered orbital phase of 0.29–0.47, and we found also that the iron line energy varied with the orbital phase. This information is useful to constrain the reprocessing site of the iron line emission. We discuss first the variations of the iron line parameters with the orbital phase and then iron line pulsation and the line energy variation with the pulse phase.

4.1. *Pulse-averaged Properties*

We obtained an average iron line energy of 6.46 ± 0.05 keV. Previous observations of the iron line with *Tenma* (6.42 ± 0.02 keV; Nagase et al. 1986) and *EXOSAT* (6.37 ± 0.10 keV and 6.51 ± 0.12 keV; Haberl & White 1990) are consistent with the present results. As mentioned in § 3, multiple iron lines (e.g., 6.42 keV Kα line, 6.68 keV He-like Kα line, and 7.06 keV Kβ line) were detected in the eclipse spectrum of Vela X-1 with the *ASCA* SIS (Nagase et al. 1994). Among these, the 6.4 keV line was the most prominent. Thus, it is natural to assume that the iron line we observed is in fact multiple and is not resolved by the *Ginga* LAC. The case is the same for the *Ginga* and *ASCA* observations of Cen X-3 (Ebisawa et al. 1996), which also show a single line in the former and multiple lines in the latter. The variations of the line center energy among the data sets A through D and over pulse phase are considered due to the change of the relative contribution of the various iron lines that may be due to time and site-dependent changes of ionization degree of the X-ray–irradiated stellar wind.

Although we detected a nonzero width for the iron line from all four data sets, caution must be adopted in its interpretation. The selection of the continuum model (including the K-shell absorption edge of iron) is crucial to investigating the line width with low-energy resolution detectors such as the LAC. Hence, we tried first to change the K-shell absorption edge energy of iron and its depth around 7.1 keV to see how the line width is affected. We found that a broad line was always necessary even if the edge energy and depth were freed in the course of model fitting. Next we tried a different continuum model, i.e., the one adopted by Mihara (1995) $[(I_1 E^{-\alpha_1} + I_2 E^{+\alpha_2}) \exp(-E/kT)]$. The results on line width were same within the statistical error, and we needed a broad line. From these investigations, we can say that the broad line we obtained is not an artifact due to the particular choice of model. Using the *Tenma* data, Ohashi et al. (1984) set an upper limit of the iron line width of 0.5 keV (FWHM), and Nagase et al. (1986) set those of 0.4–0.8 keV for various Vela X-1 data sets. On the other hand, according to the iron line catalog of the *EXOSAT* GSPC (Gottwald et al. 1995), the iron line width of Vela X-1 changed from being narrow to a value of 1.6 keV. Recent *ASCA* observations throughout an eclipse transition revealed multiple lines, but these are consistent with narrow lines (Nagase et al. 1994). Considering these observations, the iron line parameters of Vela X-1 may vary with time and may depend on orbital phase. Although the present analysis indicates a broad iron line, we feel that high-resolution spectroscopic observations, such as those by *ASCA* at different orbital phases, are essential to draw clear conclusions on the line width.

The equivalent width of the iron line was almost constant at ~ 0.3 keV when the absorption column was moderate and increased up to 1.3 keV with the high column of log $N_{\rm H} = 24.35$. A similar tendency was observed previously with *Tenma* (Nagase et al. 1986), although the equivalent width was smaller on average than the present observations. The difference in equivalent width may result from the finite line width of our data. The increase of the iron equivalent width at large column is consistent with the tendency expected from a spherically symmetric distribution of matter.

The phase-averaged line energy of 6.58 ± 0.07 keV at the orbital phase 0.45 (D) is significantly larger than the 6.4 keV fluorescent energy. A significant contribution of He-like (and possibly H-like) iron should be present in at least some of this data set. It has been established that the ionization degree of the reprocessing matter is characterized by the ξ parameter defined as $\xi = L_{\rm X}/n_e r^2$ (n_e is the electron number density of the local gas and r is the distance from the neutron star). The ξ parameter should be larger than a few hundreds to ensure that He-like iron is present at some fraction. This means that the ξ parameter of X-ray reprocessing site is supposed to range from less than about 100 (data sets A and C) to at least a few hundreds (data set D). If $n_e r$ is assumed to be equal to the absorption column density, and we use the average X-ray luminosity of 3×10^{36} ergs s^{-1}, then the distance to the reprocessing site from the neutron star would be of order $\sim 10^{11}$ cm. A reprocessing site at this distance is expected to be occulted during the eclipse. In fact, the iron line flux observed during the eclipse phase, 3.6×10^{-4} photons cm^{-2} s^{-1} (Nagase et al. 1994), is an order of magnitude smaller than that obtained from the present analysis (Table 1). This supports the above conjecture that the iron line emission site is located $\sim 10^{11}$ cm from the neutron star.

One of the possible reprocessing sites around 10^{11} cm from the neutron star is an accretion wake (Blondin et al. 1990). Of the alternative sites, a photoionization wake cannot plausibly produce iron fluorescent lines at orbital phases less than 0.5 (Kaper, Hammerschlag-Hensberge, & Zuinderwijk 1994). The companion star atmosphere is also unplausible because its distance from the neutron star (1.3×10^{12} cm) is an order of magnitude larger than the current estimation. The gas density in the accretion wake can be 100 times as large as that of the stellar wind and may be enough to explain the hydrogen column density of order 10^{23} cm^{-2} (Blondin et al. 1990). Large absorption columns tend to appear at $\Phi_{\rm orb} > 0.5$, but episodic increases may be possible even at smaller orbital phases due to the nonsteady nature of the accretion wake. Furthermore, an accretion wake can cover a large solid angle around the neutron star, which may be enough to produce the observed equivalent width of the iron line. Thus, the accretion wake is the most promising site of the iron line reprocessing.

4.2. *Pulse-resolved Properties*

The results we obtained on the iron line from the pulse phase–resolved spectroscopic analysis may be explained consistently by X-ray reprocessing at the accretion wake.

We detected significant modulation of the iron line flux with pulse period from data set B. The amplitude of the modulation was about 10%. We note here that this amplitude is much smaller than that of the intrinsic beam above

7.1 keV (i.e., ~60% of data set D, as seen in Figure 2). Although Ohashi et al. (1984) failed to detect significant modulation of the iron line flux, the above result is consistent with that of Ohashi et al. within their statistical limit. The presence of the modulation indicates that the distribution of the reprocessing matter is not completely spherically symmetric around the neutron star. The matter should be distributed anisotropically, producing the iron flux modulation. Although the accretion wake covers nearly π around the neutron star, its matter distribution is clearly not spherically symmetric. Anisotropy of the absorbing column as viewed from the neutron star may be responsible for the iron line modulation.

The pulse phase at which the iron line flux reaches its maximum in data set B coincides with the main peak of the continuum above 7.1 keV (Fig. 4). This means that a major part of the reprocessing matter is located on the line of sight. X-rays that experience the largest absorption column are those traveling along the boundary of the accretion wake. Such a direction may almost coincide with the line of sight. It may be noteworthy that the iron line modulation seems to have a single-peaked pulse profile, while the continuum has a double-peaked profile. Therefore, only one of the two X-ray beams may cross the high column direction of the accretion wake.

We detected a clear modulation of the iron line energy in data set D. The iron line energy changed from 6.4 to 6.8 keV. This means that iron in reprocessing matter is dominated by He-like ions at the pulse phase 0.1–0.4 and is dominated by neutral or low ionization ions at the other pulse phases. The phase 0.1–0.4 coincides with the main peak of the pulse profile (Fig. 2). Thus, the X-ray beam from the pulsar is considered to be directed toward us. The data set D corresponds to the orbital phase 0.43–0.47, and we may be looking at the neutron star through the tail of the accretion wake. The plasma inside the accretion wake, which experiences the bow shock, is expected to have high temperature and low density. This means that the ξ parameter inside the accretion wake can be higher than outside. The relatively high X-ray flux due to the main peak of the pulsation also pushes the ξ parameter to higher values. These effects may explain the He-like ionization state of iron in pulse phase 0.1–0.4. Outside this pulse phase, the X-ray beams are reprocessed mainly by the undisturbed stellar wind, and hence the ionization state of iron is relatively low. Similarly, since the iron is close to neutral in the other data sets and does not show large variations over the pulse phase, it is suspected that the X-ray beam from the pulsar may not travel long inside the accretion wake.

5. SUMMARY AND CONCLUSIONS

Ginga data of Vela X-1 (4U 0900−40) were analyzed, paying attention to the iron line to investigate the circumstellar matter in the binary system. The main findings in this study are summarized as follows:

1. The line energy derived from pulse-averaged spectra ranged from 6.36 to 6.58 keV and the equivalent width from 0.24 to 1.31 keV depending on the absorption column. These results are consistent with previous observations.
2. Clear modulation of the iron flux with the pulse period is observed at the half-amplitude of 10% during the intensity dip at $\Phi_{\rm orb} = 0.33$–0.38. The pulse phase at which the iron line flux reaches its maximum coincides with the main peak of the continuum above 7.1 keV.
3. Clear modulation of the iron line energy between 6.4 and 6.8 keV is detected at $\Phi_{\rm orb} = 0.43$–0.47. All these findings can be explained consistently by X-ray reprocessing in the accretion wake. The absorption column of the accretion wake can exceed $\log N_{\rm H} = 24$ and may subtend a solid angle $\sim\pi$ when viewed from the neutron star. Anisotropy of the matter distribution of the accretion wake may be responsible for the iron line modulation with the pulse period. Emission lines from highly ionized iron may be produced by hot thin plasma inside the accretion wake, which has been bow shocked.

The authors wish to thank all the members of the *Ginga* team for these observations. The present study was supported in part by the basic research projects 94-5100-005 and 96-5200-002 of the Korea Astronomy Observatory.

REFERENCES

Anzer, U., Börner, G., & Monaghan, J. J. 1987, A&A, 176, 235
Becker, R. H., Rothschild, R. E., Boldt, E. A., Holt, S. S., Pravdo, S. H., Serlemitsos, P. J., & Swank, J. H. 1978, ApJ, 221, 912
Blondin, J. M., Kallman, T. R., Fryxell, B. A., & Taam, R. E. 1990, ApJ, 356, 591
Blondin, J. M., Stevens, L. R., & Kallman, T. R. 1991, ApJ, 371, 684
Börner, G., Hayakawa, S., Nagase, F., & Anzer, U. 1987, A&A, 182, 63
Boynton, P. E., Deeter, J. E., Lamb, F. K., Zylstra, G., Pravdo, S. H., White, N. E., Wood, K. S., & Yentis, D. J. 1984, ApJ, 283, L53
Chodil, G., Mark, H., Rodrigues, R., Seward, F. D., & Swift, C. D. 1967, ApJ, 203, 417
Choi, C. S., Nagase, F., Makino, F., Dotani, T., Kitamoto, S., & Takahama, S. 1994, ApJ, 437, 449
Conti, P. S. 1978, A&A, 63, 225
Day, C. S. R., Nagase, F., Asai, K., & Takeshima, T. 1993, ApJ, 408, 656
Dupree, A. K., et al. 1980, ApJ, 238, 969
Ebisawa, K., Day, C. S. R., Kallman, T. R., Nagase, F., Kotani, T., Kawashima, K., Kitamoto, S., & Woo, J. W. 1996, PASJ, in press
Fransson, C., & Fabian, A. C. 1980, A&A, 87, 102
Gottwald, M., Parmar, A. N., Reynolds, A. P., White, N. E., Peacock, A., & Taylor, B. G. 1995, A&AS, 109, 9
Gottwald, M., & White, N. E. 1990, in Iron Line Diagnostics, ed. A. Treves, G. C. Perola, & L. Stellar (Berlin: Springer), 134
Haberl, F., & White, N. E. 1990, ApJ, 361, 225
Kallman, T. R., & White, N. E. 1982, ApJ, 261, L35
Kaper, L., Hammerschlag-Hensberge, G., & Zuindewijk, E. J. 1994, A&A, 289, 846
Koyama, K., Makishima, K., Tanaka, Y., & Tsunemi, H. 1986, PASJ, 38, 121
Krolik, J. H., & Raymond, J. C. 1985, ApJ, 298, 660
Lewis, W., Rappaport, S., Levine, A., & Nagase, F. 1992, ApJ, 389, 665
Livio, M., Soker, N., de Kool, M., & Savonije, G. J. 1986, MNRAS, 218, 593
Makishima, K., et al. 1990, ApJ, 365, L59
McClintock, J. E., et al. 1976, ApJ, 206, L99
Mihara, T. 1995, Ph.D. thesis, Univ. Tokyo
Morrison, R., & McCammon, D. 1983, ApJ, 270, 119
Nagase, F. 1989, PASJ, 41, 1
Nagase, F., et al. 1984a, ApJ, 280, 259
———. 1984b, PASJ, 36, 667
———. 1991, ApJ, 375, L49
Nagase, F., Hayakawa, S., Makino, F., Sato, N., & Makishima, K. 1983, PASJ, 35, 47
Nagase, F., Hayakawa, S., Sato, N., Masai, K., & Inoue, H. 1986, PASJ, 38, 547
Nagase, F., Zylstra, G., Sonobe, T., Kotani, T., Inoue, H., & Woo, J. 1994, ApJ, 436, L1
Ohashi, T., et al. 1984, PASJ, 36, 699
Sato, N., et al. 1986, PASJ, 38, 731
Soker, N., Livio, M., de Kool, M., & Savonije, G. J. 1986, MNRAS, 221, 445
Taam, R. E., & Fryxell, B. A. 1989, ApJ, 339, 297
Turner, M. J. L., et al. 1989, PASJ, 41, 345
Vidal, N. V., Wickramasinghe, D. T., & Peterson, B. A. 1973, ApJ, 182, L77
Watson, M. G., & Griffiths, R. E. 1977, MNRAS, 178, 513
White, N. E., Swank, J. H., & Holt, S. S. 1983, ApJ, 270, 711